Control of Pore Size and Pore Uniformity in Films Based on Self-Assembling Block Copolymers

Erik J. Vriezekolk,[1] Eddy de Weerd,[2] Wiebe M. de Vos,[1] Kitty Nijmeijer[1]

[1]TNW, Membrane Science and Technology, Mesa$^+$ Institute for Nanotechnology, University of Twente, P.O. Box 217, 7500 AE Enschede, The Netherlands
[2]EWI, BIOS Lab on a Chip, University of Twente, P.O. Box 217, 7500 AE Enschede, The Netherlands
Correspondence to: W. M. de Vos (E-mail:w.m.devos@utwente.nl)

Received 21 July 2014; accepted 11 September 2014; published online 3 October 2014
DOI: 10.1002/polb.23600

ABSTRACT: Blends of self-assembling polystyrene-*block*-poly(4-vinyl pyridine) (PS-*b*-P4VP) diblock-copolymers and poly(4-vinyl pyridine) (P4VP) homopolymers were used to fabricate isoporous and nanoporous films. Block copolymers (BCP) self-assembled into a structure where the minority component forms very uniform cylinders, while homopolymers, resided in the core of the cylinders. Selective removal of the homopolymers by ethanol immersion led to the formation of well-ordered pores. In films without added homopolymer, just immersion in ethanol and subsequent swelling of the P4VP blocks was found to be sufficient to create pores. Pore sizes were tuned between 10 and 50 nm by simply varying the homopolymer content and the molecular weight of the block-copolymer. Uniformity was lost when the average pore size exceeded 30 nm because of macrophase separation. However, preparation of films from low M_W diblock copolymers showed that it is possible to have excellent pore size control and a high porosity, while retaining a low pore size distribution. © 2014 Wiley Periodicals, Inc. J. Polym. Sci., Part B: Polym. Phys. **2014**, *52*, 1568–1579

KEYWORDS: block copolymers; homopolymers; isoporous and nanoporous films; membranes; self-assembly; tuning pore sizes

INTRODUCTION Spontaneous self-assembly of block copolymers (BCPs) has gained a lot of interest, since these polymers have the ability to form periodically well-ordered structures with sizes in the nanometer range.[1] Depending on their nature, composition and size, block copolymers can self-assemble into various types of nanostructures, for example, spherical, lamellar, and cylindrical.[2–4] Thin films made of block copolymers having a morphology of hexagonally packed cylinders perpendicular to the film surface are promising for use in several applications, for example, ultrafiltration (UF) membranes,[5–7] antireflection coatings, and drug delivery,[8] since removal of the minority component that forms the cylinders leads to a film with a very narrow pore size distribution. Ordered structures of block copolymers can also be used as a template for preparing nanoarrays[9,10] or as a mask for nanopatterning[11] after selectively removing one of the domains. In addition, it can be used as a template for porous inorganic materials by mixing block copolymers and inorganic species and subsequently removing the BCPs by calcination.[12–14]

Fabrication of block copolymer-based nanoporous structures can be divided into three strategies. In the first approach, a film is made where block copolymers self-assemble into a nanostructure. Subsequently, a minority component is selectively removed by, for example, etching.[15–21] Because the formation of the nanostructure is based on equilibrium, very ordered structures can be obtained after a thermal or solvent annealing step.[22–29] However, the pore size is determined only by the size of the minority component and is typically only in the range of 5–55 nm,[20] depending on the nature of the copolymers,[30] which reduces the range of applicability for separations. A second strategy is the direct formation of pores by *phase inversion*.[31–34] Here, a polymer which is initially dissolved in a solvent, rapidly solidifies due to a fast exchange between the solvent and a nonsolvent.[35] This results in a structure where the block copolymers are kinetically frozen in a nanoporous matrix. Although this technique does not require a subsequent step in order to create pores, it has some drawbacks: first, a large amount of block copolymers is required to fabricate films, since most of the block copolymer is used to fabricate a thick support layer. Second, it is difficult to tune the pore sizes. A third strategy to create nanoporous films is to add a sacrificial component to the system that is later removed by rinsing, thereby creating pores.[8,36–39] The idea is that this additional component, that is, a homopolymer (HP), will reside in the nanodomain of one of the copolymer blocks because of preferential

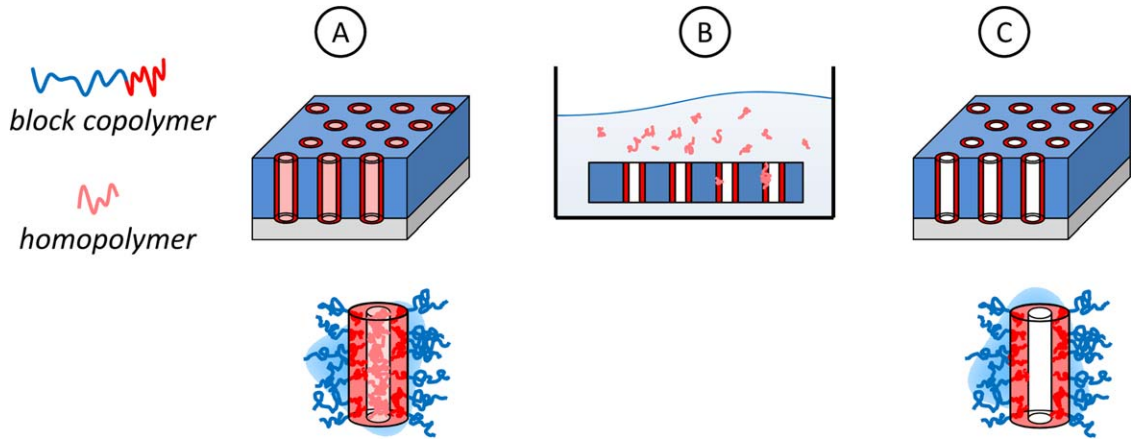

FIGURE 1 Schematic overview of the fabrication of nanoporous layers. (a) A PS-*b*-P4VP block copolymer/$P4VP_{HP}$ homopolymer film is made by spincoating a PS-*b*-P4VP/$P4VP_{HP}$ solution on a silicon substrate. The block copolymers self-assemble in a hexagonal cylindrical structure perpendicular to the surface, where the homopolymers reside in the cylinders. Subsequent removal of the homopolymer with a solvent rinse (b) leads to a film with uniform and straight-through nanopores (c). [Color figure can be viewed in the online issue, which is available at wileyonlinelibrary.com.]

interactions between this polymer block and the additional component. With this technique, pore sizes can be tuned by simply adjusting the content of the homopolymer for films with perpendicularly orientated cylinders,[36] and pore sizes can be obtained that are smaller than achievable with pure block copolymer films.[40] However, while adding a small fraction of homopolymers can enhance the ordering of cylinders,[41,42] larger additive fractions that are required to create pores come at a cost of pore size distribution, since the desired structure of uniformly distributed homopolymers will not be an equilibrium structure, but a kinetically trapped structure.[36]

For the combination of BCPs and HPs, much research has focused on the orientation of the BCP nanodomains or the involved phase separation mechanisms.[43–53] Furthermore, the removal of HPs by UV-radiation rather than by selective solvents has been carefully investigated.[54] However, the precise control of pore sizes and porosities, using the selective solvent approach, has not been investigated thoroughly. This is somewhat surprising, as understanding and control over this final step, were the nanoporous, straight-through films are fabricated, is key for various applications, for example, membrane technology.

This paper presents a very detailed investigation into the fabrication of nanoporous, isoporous films using a block copolymer/homopolymer system by removing the HP with a selective solvent. We show that a combination of HP removal by solvent and swelling of BCP determine the pore size and porosity, especially at smaller pore sizes. While pore formation by UV radiation does not change the nanodomain periodicity of the film,[55] HP removal by a solvent does change the nanodomain sizes and periodicities by swelling.

We focus on understanding strategies to tune the pore size and porosity, while keeping the pore size distribution low, by varying process parameters during the fabrication of films. The thin films under investigation are based on asymmetric polystyrene-*b*-poly(4-vinyl pyridine) (PS-*b*-P4VP) block copolymers and poly(4-vinyl pyridine) ($P4VP_{HP}$) homopolymers. PS-*b*-P4VP is a block copolymer that is commonly used and studied[36,56,57] because of its excellent self-assembly properties. In our work, the block copolymers self-assemble into a hexagonal cylindrical nanostructure, where the P4VP blocks form cylinders and the P4VP homopolymers are situated inside these cylinders [Fig. 1(a)]. Subsequent selective removal of $P4VP_{HP}$ leads to the formation of uniform and straight-through nanopores [Fig. 1(b)].

The molecular weight of the block copolymer, the content and molecular weight of the homopolymers and the procedure for selective removal of the homopolymer are varied in order to investigate their effects on the formed morphology. Additionally, the effect of solvent vapor exposure of the fabricated films is investigated as a method to enhance the ordering and uniformity of the pores.

EXPERIMENTAL

Materials

Polystyrene-*b*-poly(4-vinyl pyridine) (PS-*b*-P4VP) block copolymers P5546P-S4VP (M_w = 160-*b*-21 kg/mol, PDI = 1.07), P3910A-S4VP (M_w = 109-*b*-30 kg/mol, PDI = 1.15), and P4829P-S4VP (M_w = 50-*b*-13 kg/mol, PDI = 1.05) and poly(4-vinyl pyridine) homopolymers P8285-4VP (M_w = 22 kg/mol, PDI = 1.16), P8284-4VP (M_w = 11 kg/mol, PDI = 1.15), and P3414-4VP (M_w = 5.2 kg/mol, PDI = 1.20) were all purchased from Polymer Source, Canada. All polymers were used without further purification. Chloroform, acetone, and ethanol (all of analytical grade) were purchased from Sigma Aldrich.

Preparation of Nanoporous Films

PS-*b*-P4VP block copolymers and P4VP homopolymers were dissolved in chloroform and stirred for several hours at

TABLE 1 Film Fabrication Process Parameters that were Varied During Experiments

BCP (kg/mol)	HP (kg/mol)	$f_{P4VP\text{-}HP}$[a]	$f_{P4VP\text{-}total}$[b]	Ethanol Immersion Time (h)
160-*b*-21	22	**0–0.31**	**0.12–0.39**	2.5
109-*b*-30	22	**0.10**	**0.29**	2.5
50-*b*-13	22	**0.04–0.35**	**0.23–0.48**	2.5
160-*b*-21	**5; 11; 22**	0.16	0.26	2.5
160-*b*-21	22	0.21	0.30	**10 s to 2.5 h**

Names and values in bold show the range in which the parameter is varied.

[a] Weight fraction of P4VP homopolymers of the total polymer content.

[b] Weight fraction of BCP P4VP chains and P4VP homopolymers of the total polymer content.

room temperature. The total polymer concentration (block copolymer + homopolymer) was kept constant at 2 wt %, while the total polymer weight fraction of the homopolymers was varied between 0 and 0.35. Thin films were prepared by spincoating a polymer solution on a 2 × 2 cm silicon wafer with a native oxide layer of several nanometers, which was cleaned with acetone before use. The coverage of solution on the wafer prior to spincoating was ~0.1 ml/cm^2. Spincoating was performed at 2000 rpm for 1 min in nitrogen environment at room temperature. To obtain nanopores, the films were subsequently immersed in ethanol for different durations (10 s to 2.5 h) to dissolve and rinse away the homopolymers.

Chloroform was chosen as a solvent because it dissolves both polystyrene and poly(4-vinyl pyridine). Interaction parameters of chloroform and the polymer blocks are $\chi_{\mathrm{chloroform-PS}} = 0.10$ and $\chi_{\mathrm{chloroform-P4VP}} = 0.15$,[58] which indicates a good solvent quality of chloroform towards both blocks. Ethanol is chosen because it dissolves poly(4-vinyl pyridine) but not polystyrene, which makes it possible to selectively remove the homopolymers without significantly modifying the block copolymer film.

Different types of nanoporous films were fabricated by adjusting materials and/or process conditions during fabrication. An overview of these parameters of all fabricated nanoporous films is presented in Table 1.

Some films (PS(160)-*b*-P4VP(21)/P4VP$_{HP}$(22), $f_{P4VP\text{-}HP} = 0.21$) were also given a chloroform vapor annealing treatment, which took place prior to or after immersion in ethanol. Films were placed in a closed Petri dish that was saturated with chloroform vapor at room temperature for different durations (0.5 to 4 h).

Characterization

Atomic force microscopy (AFM, Digital Instruments) was used to visualize and characterize the surface of the films. A nanosensors SSS-NCH probe with supersharp tip (tip radius <2 nm) was used as AFM probe. Ellipsometry (Spectroscopic Ellipsometer M-2000X, J.A. Woolam, light reflection at 70°, spot size of 2 mm in diameter, wavelength range of 600–1000 nm) was used to determine the thickness of the films.

The average pore diameter, surface porosity, and domains per μm^2 were determined from three or four 1 μm × 1 μm AFM images from a minimum of two samples. The error in pore diameter was calculated using standard rules for error propagation.

RESULTS AND DISCUSSION

For clarity, block copolymers are denoted as PS(*x*)-*b*-P4VP(*y*), where *x* and *y* are the molecular masses (in kg/mol) of the PS block and P4VP block, respectively. P4VP homopolymers are denoted as P4VP$_{HP}$(*z*), where *z* is the molecular mass of the homopolymer (in kg/mol). The term *surface porosity* is defined as the fraction of the film surface covered by pores. All fabricated films had a thickness of 282 ± 34 nm.

Tuning Pore Sizes by Varying Homopolymer Content and Block Copolymer Size

Initially, films were fabricated without the addition of homopolymers. It is known that a nanoporous structure can be obtained by immersing a film of PS-*b*-P4VP micelles in ethanol.[59] Ethanol selectively swells the P4VP micellar core, which in turn pushes the PS corona's together to form a continuous film. Upon drying, the P4VP deswells and pores are formed of about 30–50 nm and with a high polydispersity.[59] We investigated if ethanol immersion would also create pores in a dense PS-P4VP film. Figure 2 shows AFM height images of a PS(160)-*b*-P4VP(21) film before and after immersion in ethanol. Before immersion in ethanol the film shows small dots. The dots are the cylindrical P4VP nanodomains seen from above, which are elevated several nanometers with respect to the flat surface. After immersion in ethanol small pores can be seen instead with an average diameter of 10.2 ± 2.6 nm. This indicates that just immersion in ethanol indeed creates nanopores within the pure block copolymer film. In contrast to the micellar approach mentioned earlier, the film remains well ordered and has a very low pore size distribution.

Figure 3 shows AFM pictures of PS(160)-*b*-P4VP(21) films made from 2 wt % polymer/chloroform solutions with different weight fractions of P4VP$_{HP}$(22). The dark dots seen on the AFM images are the pores. Comparing Figure 3(a–c) shows that larger pores are obtained when a higher P4VP$_{HP}$

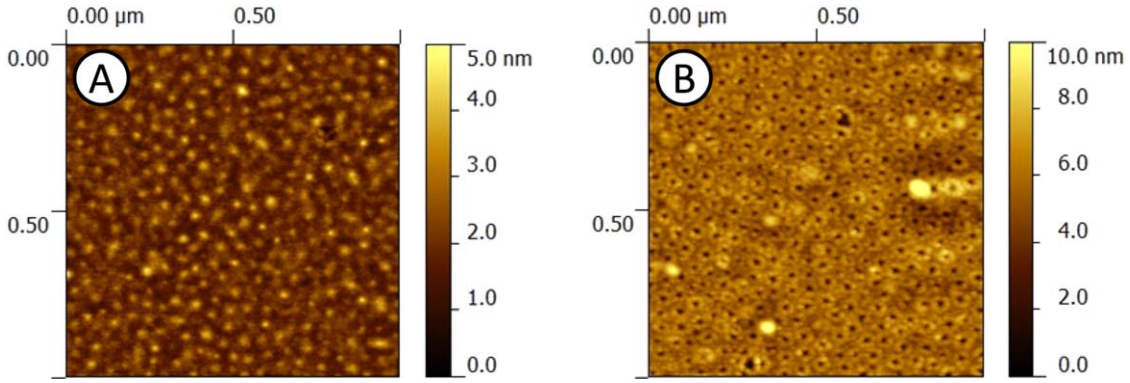

FIGURE 2 AFM height images of a PS(160)-*b*-P4VP(21) film before (a) and after (b) immersion in ethanol for 2.5 h. [Color figure can be viewed in the online issue, which is available at wileyonlinelibrary.com.]

content is used, which implies that the pore size can be tuned by simply varying the amount of $P4VP_{HP}$. Apparently, when a higher $P4VP_{HP}$ content is used larger HP domains are formed and after the homopolymer is rinsed away, this leads to larger pores. As was demonstrated earlier, also swelling of the BCP P4VP chains in ethanol can create pores, which could contribute significantly to the formation of pores when low amounts of homopolymers (=smaller pores) are used. However, it is also possible that the voids that are created by the removed homopolymers provide enough space for the BCP P4VP chains to swell. In this case, swelling of the BCP P4VP chains would not contribute to pore formation anymore. Further on in this paper we will come back to this, when we discuss the porosity of the formed layers.

Figure 3(a–c) also shows that a higher $P4VP_{HP}$ content also leads to less uniform pore sizes, that is, a higher pore size distribution. A $P4VP_{HP}$ fraction of 0.31 [Fig. 3(a)] leads to a structure with several large pores of >100 nm and smaller pores in the range of tens of nanometers. When the $P4VP_{HP}$ content is decreased, also the pore size distribution decreases (Fig. 3). The formation of the cheese-like structure

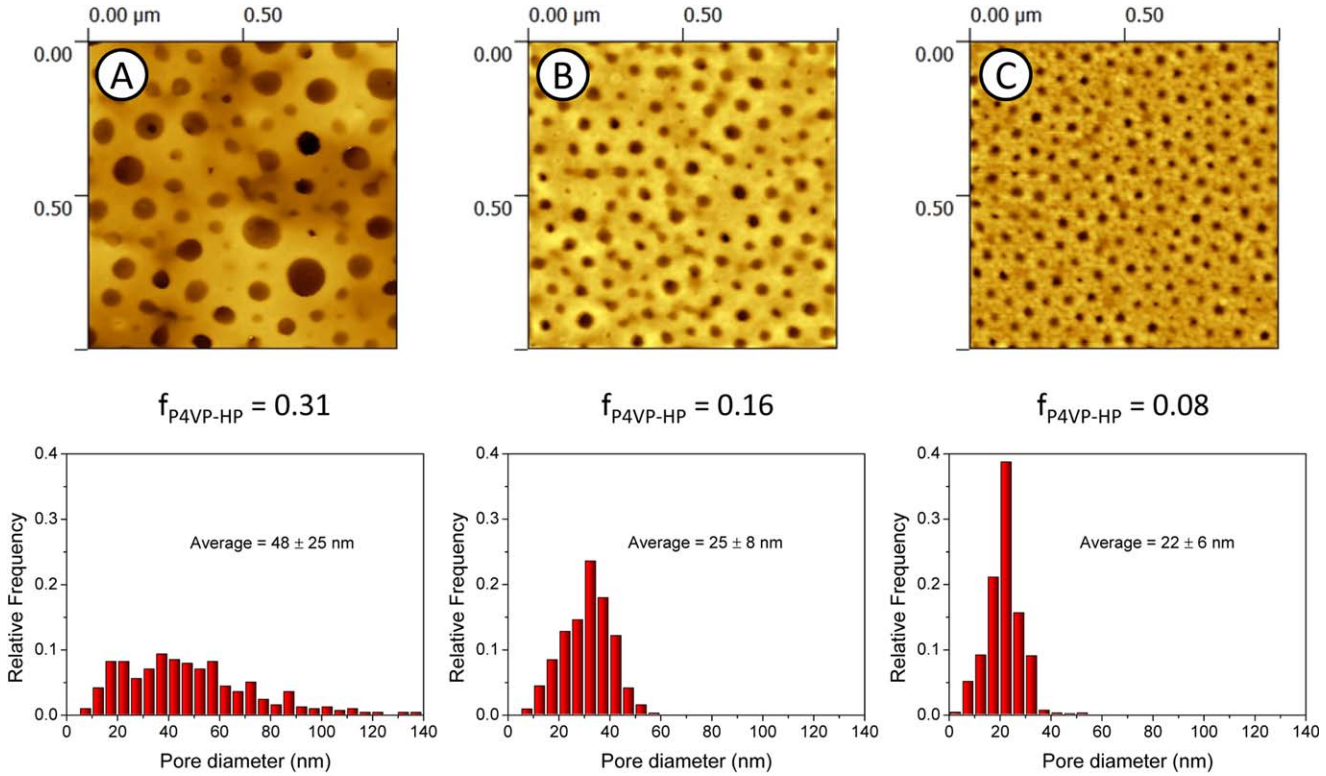

FIGURE 3 AFM height images and relative pore diameter frequencies of films made of PS(160)-*b*-P4VP(21)/$P4VP_{HP}$(22) blends using $P4VP_{HP}$ weight fractions of (a) 0.31, (b) 0.16, and (c) 0.08. [Color figure can be viewed in the online issue, which is available at wileyonlinelibrary.com.]

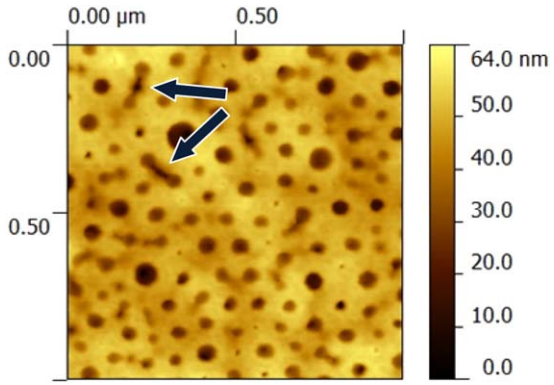

FIGURE 4 AFM height image of a film made with a PS(160)-*b*-P4VP(21)/P4VP$_{HP}$(22) blend using a P4VP$_{HP}$ weight fraction of 0.20. The arrows show gutters on the surface that connect several pores. This phenomenon was observed in films when a P4VP$_{HP}$ fraction higher than 0.15 was used together with this block copolymer. [Color figure can be viewed in the online issue, which is available at wileyonlinelibrary.com.]

of the film made with P4VP$_{HP}$ = 0.31 [Fig. 3(a)] has been defined as *macrophase separation*, while the formation of more isoporous and ordered structures seen using lower P4VP$_{HP}$ values has been defined as microphase separation.[55] To explain this, we consider two competing mechanisms to occur during solidification of the polymers and structure formation.

First, the thermodynamically driven self-assembly of the block copolymers that forms the well-ordered equilibrium nanostructure, and second, the solidification of the P4VP$_{HP}$ that tends to form larger domains in order to minimize the surface area. At low P4VP$_{HP}$ fractions, the effect of the self-assembly of BCP's dominates, and since P4VP$_{HP}$ has a favorable interaction with the P4VP blocks of the block copolymer they will distribute along the cylindrical nanodomains. However, at higher P4VP$_{HP}$ fractions the influence of the self-assembly of the block copolymers becomes less and the formation of larger sized P4VP$_{HP}$ domains occurs, which results in a larger pore size distribution and eventually macrophase separation. When the fraction of P4VP$_{HP}$ exceeded 0.15, also small gutters that connect two or more pores can be seen on the surface, as shown in Figure 4. These gutters are most likely also formed by P4VP$_{HP}$ segregated from the block copolymer nanodomains as a result of macrophase separation.

Although the pore uniformity is high using low homopolymer fractions, the pores are less ordered than the ordering of cylindrical domains usually seen in films made from pure block copolymers. It seems that the pore size distribution caused by the distribution of homopolymer over the block

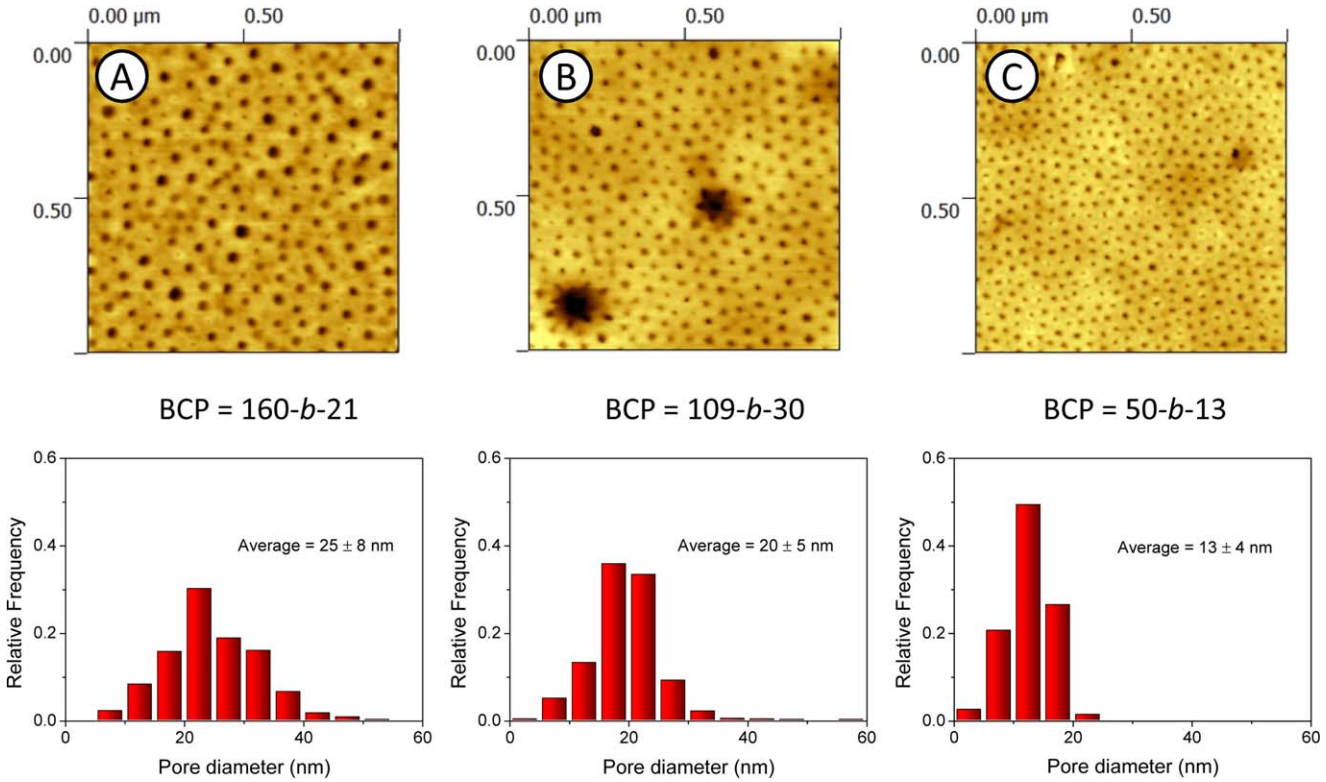

FIGURE 5 AFM height images and relative pore diameter frequencies of films made of PS-*b*-P4VP/P4VP$_{HP}$ blends using the same P4VP$_{HP}$(22) content ($f_{P4VP\text{-}HP}$ = 0.1) but different BCPs: (a) PS(160)-*b*-P4VP(21), (b) PS(109)-*b*-P4VP(30), and (c) PS(50)-*b*-P4VP(13). [Color figure can be viewed in the online issue, which is available at wileyonlinelibrary.com.]

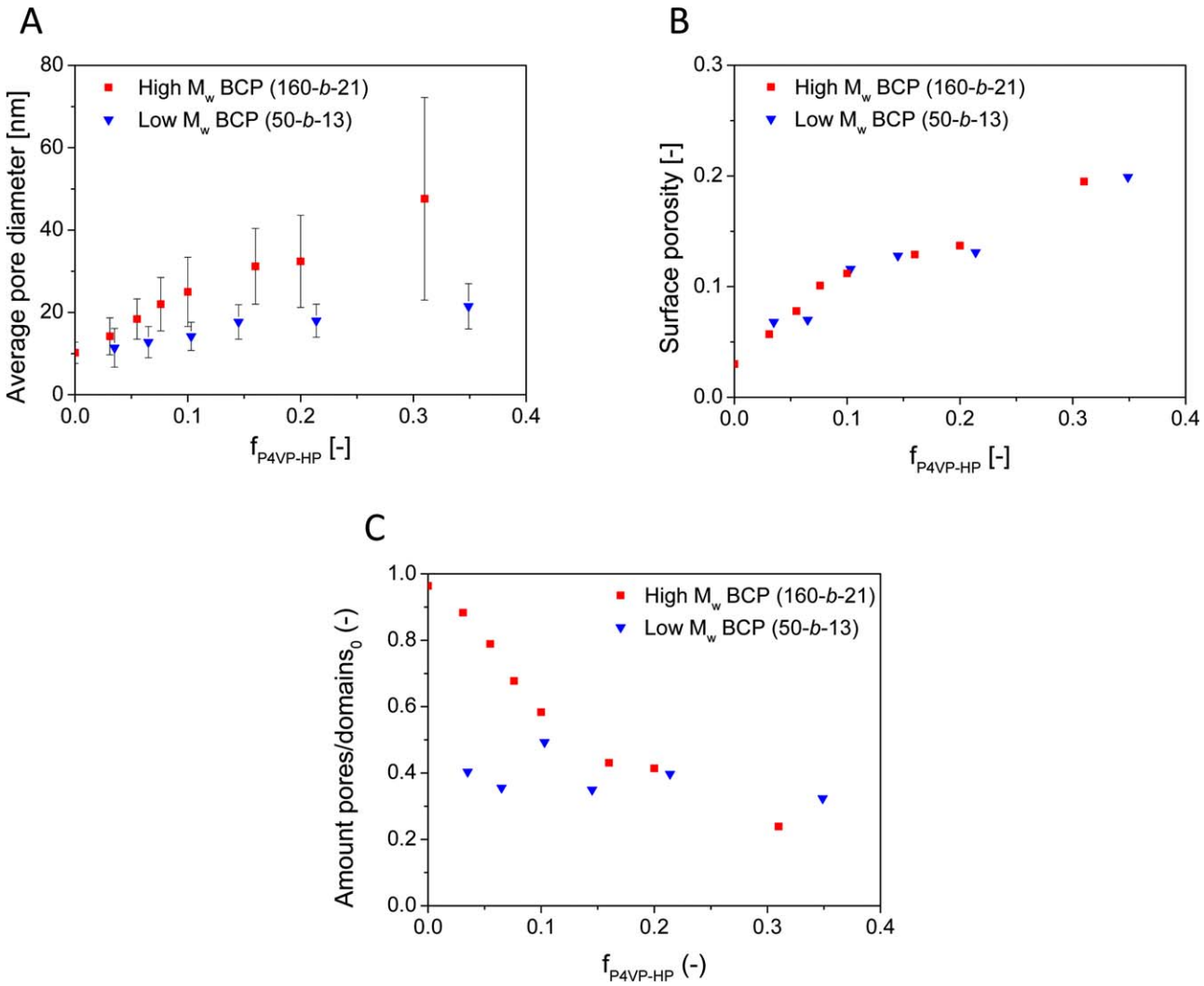

FIGURE 6 Average pore diameter (a), surface porosity (b) and amount of pores per μm^2 normalized by the amount of block copolymer domains per μm^2 without $P4VP_{HP}$ addition (c) for PS(160)-*b*-P4VP(21) (■), and PS(50)-*b*-P4VP(13) (▼) films as function of the polymer weight fraction of $P4VP_{HP}$. Note that the error bars in (a) show the standard deviation, a measure for the pore size distribution, the error in the average pore size (standard deviation in the average) is always smaller than the used symbol). [Color figure can be viewed in the online issue, which is available at wileyonlinelibrary.com.]

copolymer domains, although small, still leads to a less ordered arrangement of the pores.

Similar studies of fabricating films with PS-*b*-P4VP/$P4VP_{HP}$ blends and subsequently removing the $P4VP_{HP}$ to create pores were performed with the lower M_w PS(109)-*b*-P4VP(30) and PS(50)-*b*-P4VP(13) block copolymers. Figure 5 shows that films with significantly smaller pore sizes are obtained with PS(109)-*b*-P4VP(30) and PS(50)-*b*-P4VP(13) than with PS(160)-*b*-P4VP(21) using the same homopolymer content. Also, the pores of the lower M_w block copolymers seem more ordered and monodisperse. This demonstrates that the average pore size and pore size distribution are not only dependent on the fraction of $P4VP_{HP}$, but also on the molecular weight of the block copolymer. Smaller block copolymers self-assemble into smaller nanodomains, and since the amount of nanodomains per μm^2 is higher for smaller nanodomains, homopolymers can distribute themselves along more cylindrical nanodomains. When the homopolymers are then rinsed away, the result is smaller pores. A very promising feature is that no macrophase separation was observed in the $f_{P4VP\text{-}HP}$ range of 0.04–0.35 using the lower M_w PS(50)-*b*-P4VP(13), while it did occur for the higher M_w PS(160)-*b*-P4VP(21) block copolymer using homopolymer fractions larger than 0.16. This implies that the transition from microphase separation to macrophase separation not only depends on the molecular weight and fraction of the homopolymer (as demonstrated previously[55]), but also on the size of the block copolymer. It is likely that the effect of the block copolymers to form well-ordered nanodomains remains dominant over a larger range of $f_{P4VP\text{-}HP}$ values for smaller block copolymers, since smaller block copolymers produce smaller pores. Thus, with these smaller diblock copolymers, it is possible to create films with a very

controlled pore size, a low pore size distribution and a high porosity.

The correlation between the fraction of $P4VP_{HP}$ and the pore diameter for the systems with the large and small BCP is displayed in Figure 6(a). Both systems show a clear trend and a higher $P4VP_{HP}$ content leads to larger pores and a higher pore size distribution (larger error bars). Pores with average diameters between 10.2 ± 2.6 and 47.6 ± 24.6 nm were formed using the high M_w PS(160)-*b*-P4VP(21) BCP with $P4VP_{HP}$ fractions in the range of 0–0.31. Pores between 11.4 ± 4.7 and 21.5 ± 5.5 nm were formed using the low M_w PS(50)-*b*-P4VP(13) BCP with $P4VP_{HP}$ fractions in the range of 0.04–0.35. This implies that pore sizes can be tuned by varying the homopolymer content and/or the M_w of the block copolymer. However, since macrophase separation at higher $P4VP_{HP}$ content leads to a higher pore size distribution, uniformity of the pore sizes that can be obtained is limited for the bigger block copolymer.

Another important characteristic is the porosity of the films [Fig. 6(b)]. A higher $P4VP_{HP}$ content leads to a higher porosity, since more polymer is washed away to create voids. The correlation between porosity and $f_{P4VP\text{-}HP}$ are very similar for the large BCP and small BCP system, which implies that the porosity is indeed only a function of the amount homopolymers added. However, there is no linear 1 to 1 correlation between the fraction of $P4VP_{HP}$ and the porosity, as one would expect. In the first region with $f_{P4VP\text{-}HP}$ values between 0.03 and 0.1 the porosity is similar to $f_{P4VP\text{-}HP}$ or even higher, but the trend deviates from this ideal case when larger amounts of $P4VP_{HP}$ are used and lower porosities are obtained. The lower than expected porosities are most likely due to aggregation of homopolymers (macrophase separation) that form large regions on top, below or even inside the film (not visible on the surface). The "gutters" as shown in Figure 4 are an example of this. The higher porosities in the first region can be explained by swelling of the BCP P4VP chains. As mentioned before, swelling of BCP P4VP chains by ethanol creates pores of ~10.2 nm in a pure PS(160)-*b*-P4VP(21) film, which already leads to a porosity of 0.03. Therefore, the contribution of the swelling of BCP P4VP chains to the pore formation can be significant when a low $P4VP_{HP}$ content is used to create pores. Taking this contribution into account, it is likely that the porosity created by washing away homopolymers (and not solvent swelling) is always lower than the used fraction of homopolymers.

Figure 6(c) shows the normalized amount of pores per μm^2 as function of the polymer weight fraction of $P4VP_{HP}$ using PS(160)-*b*-P4VP(21) and PS(50)-*b*-P4VP(13). Here, the amount of pores per μm^2 is normalized by the amount of domains per μm^2 for a film of pure block copolymers (without $P4VP_{HP}$ addition) to take into account the effect of the pore formation ability of the pure polymer, which differs with the M_w of the polymer. For both block copolymers the amount of pores/μm^2 decreases with increasing $P4VP_{HP}$ fraction with reference to the initial amount of domains/μm^2 of the pure block copolymer film. $P4VP_{HP}$ polymers that reside in the core of the block copolymer cylinders force the block copolymer domain to expand, which results in a larger domain area (block copolymer + homopolymer) and hence, a lower amount of pores (domains) per μm^2. PS(160)-*b*-P4VP(21) has an initial amount of domains/μm^2 of 360. With the addition and subsequent removal of $P4VP_{HP}$, the amount of pores/μm^2 decreases rapidly and almost linear to 155 (0.43 normalized) at a $f_{P4VP\text{-}HP}$ of 0.16. Using larger $P4VP_{HP}$ content leads to a lower value of 86/μm^2 (0.24 normalized) for $f_{P4VP\text{-}HP} = 0.31$, but the rate of decrease of the amount of pores/μm^2 is lower. This is likely coupled to the small increase in porosity at these homopolymer ratio's [Fig. 6(b)] which was explained by part of the homopolymer (macro)phase separating on top, at the bottom or inside the polymer film. PS(50)-*b*-P4VP(13) has an initial amount of domains/μm^2 of 1410, but this amount is more than halved to 570 (0.40 normalized) when a small of $P4VP_{HP}$ ($f_{P4VP\text{-}HP} = 0.035$) is added and subsequently removed. When more $P4VP_{HP}$ is used the amount of pores keeps decreasing very slowly to 456/μm^2 for $f_{P4VP\text{-}HP} = 0.35$. The rapid decrease in domains/μm^2 in the first region of the graphs with small amounts of $P4VP_{HP}$ for both block copolymers is most likely due to the swelling of $P4VP_{block}$, which creates pores even without the addition of $P4VP_{HP}$. Especially in the case of the smaller PS(50)-*b*-P4VP(13) block copolymer this phenomenon dominates the pore formation at low $P4VP_{HP}$ amounts (however, we were not able to measure the pore sizes and amount of pores of the $f_{P4VP\text{-}HP} = 0$ film accurately due to the small pore size). At $P4VP_{HP}$ contents >0.15, the relatively low amount of pores/μm^2 also suggests that the homopolymers do not distribute equally along the block copolymer domains, although macrophase separation starts to occur at much higher $P4VP_{HP}$ fractions. This suggests that it is likely that cylindrical nanostructures without homopolymers are present in the films.

The results in this paragraph show that isoporous nanoporous films can be made by selectively removing homopolymers from ordered block copolymer/homopolymer films, or even by simply immersing a block copolymer film in ethanol. The pore sizes and porosity can be tuned by simply varying the amount of homopolymer, which makes this approach a promising method to fabricate very selective ultrafiltration membranes. However, only a range of homopolymer content can be used before the homopolymers start to macrophase separate, which dramatically increases the pore size distribution. Since also the M_w of the block copolymer influences the pore size and the range in which homopolymers microphase separate, selection of both homopolymer content and block copolymer M_w is crucial for fabricating a film with a desired pore size and porosity. We demonstrated that by using a low M_w block-copolymer, it is possible to create films with the desired controlled pore size, low pore size distribution and high porosity.

Fabrication Optimization

In this paragraph several process parameters that influence the formation of the nanoporous films are discussed: M_w of

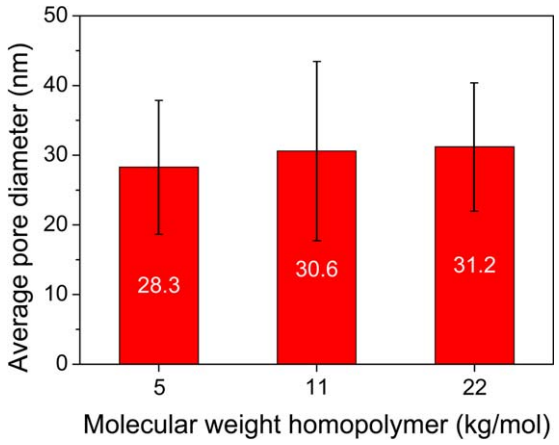

FIGURE 7 Average pore diameter of films made with PS(160)-*b*-P4VP(21)/P4VP$_{HP}$ blends using P4VP$_{HP}$ with different molecular weights. Error bars show the standard deviation, a measure for the pore size distribution. [Color figure can be viewed in the online issue, which is available at wileyonlinelibrary.com.]

used homopolymer, ethanol immersion duration and the solidification rate during the film fabrication. Also results of a solvent annealing treatment are presented and discussed.

Effect of M_w Homopolymer

PS(160)-*b*-P4VP(21) films were made from solutions with different molecular weights of homopolymers (5, 11, and 21 kg/mol), but with a fixed composition ($f_{P4VP\text{-}HP} = 0.16$). Our main interest was to investigate the effect of the M_w of the homopolymer on the pore size distribution. Figure 7 shows that the average pore diameter slightly increases when the M_w of the homopolymer is increased, but the differences fall within the experimental error (± 2 nm).

This effect was also observed for a system with polystyrene-*b*-poly(methyl methacrylate) block copolymers and poly(methyl methacrylate) homopolymers.[55] With increasing homopolymer size, one would expect an increase in pore size, as for longer chains the driving force for phase separation is stronger. However, when the pore size becomes

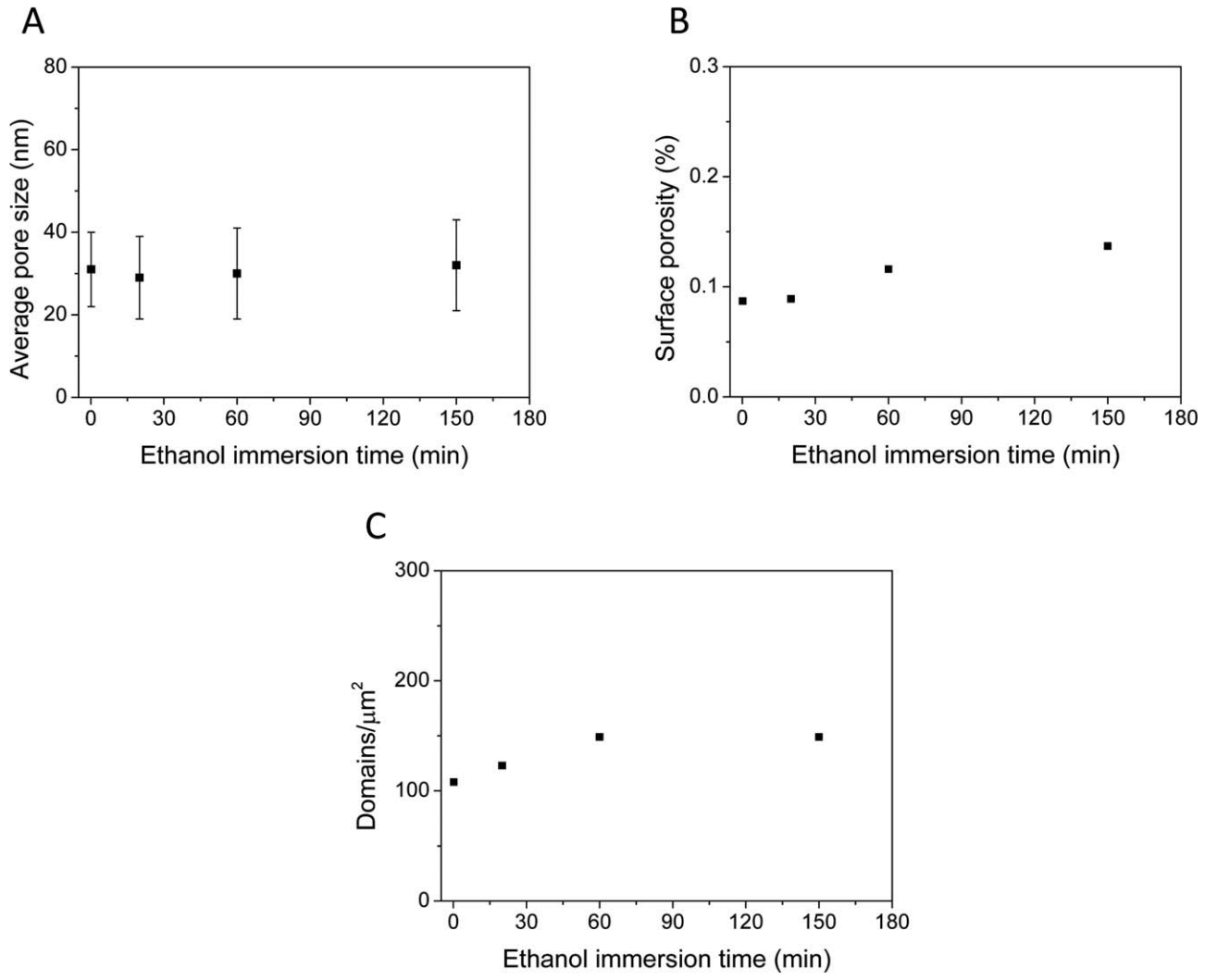

FIGURE 8 Pore size (a), porosity (b), and number of domains per μm^2 (c) as function of the ethanol immersion time using a film made of a PS(160)-*b*-P4VP(21)/P4VP$_{HP}$(22) blend with a P4VP$_{HP}$ weight fraction of 0.21.

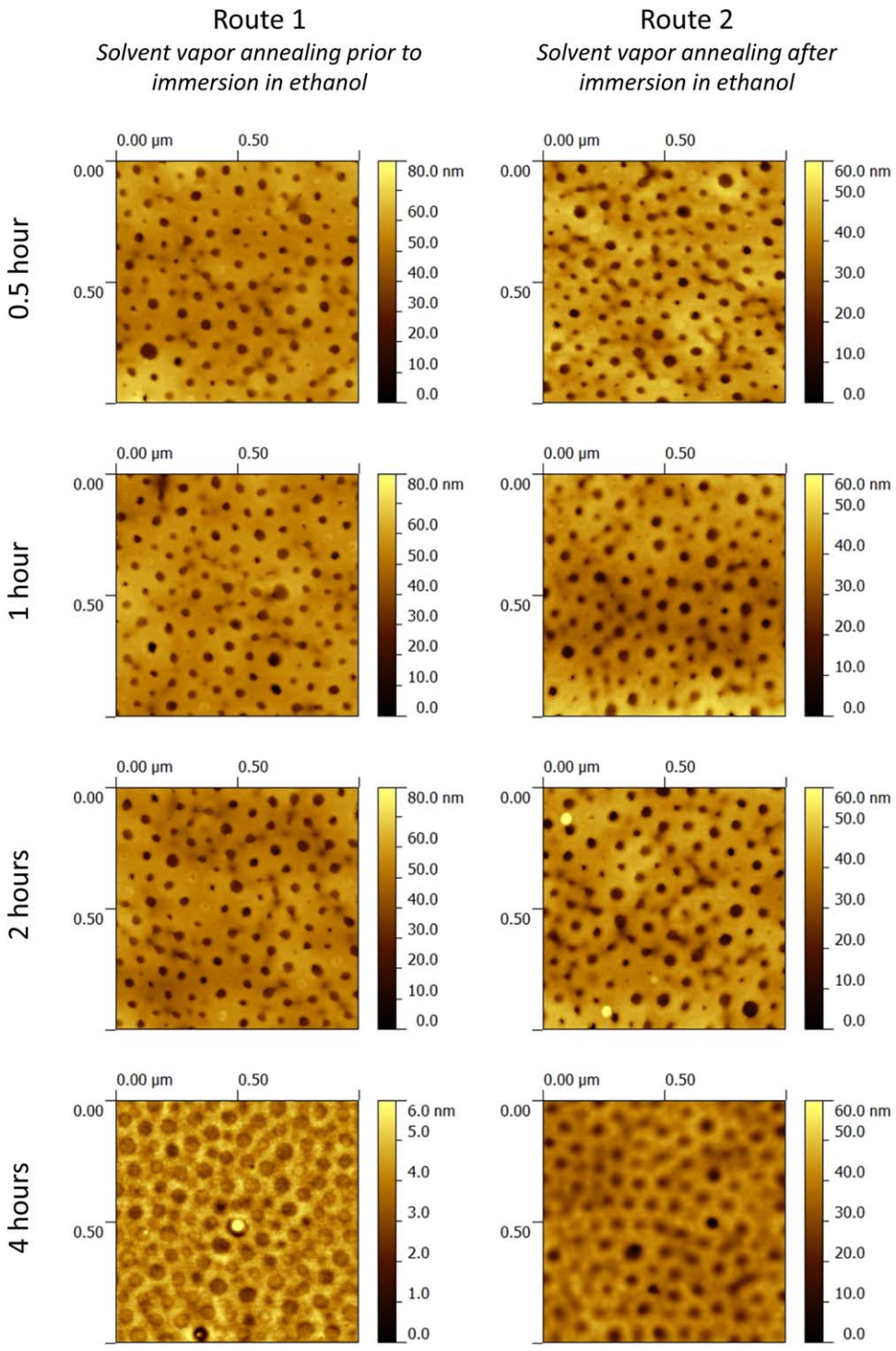

FIGURE 9 AFM height images of films exposed to chloroform vapor for different durations. Vapor annealing was performed following two routes: Prior to or after immersion of the films in ethanol. Films used where prepared from a PS(160)-*b*-P4VP(21)/$P4VP_{HP}$(22) blend with a homopolymer weight fraction of 0.21. [Color figure can be viewed in the online issue, which is available at wileyonlinelibrary.com.]

independent of homopolymer chain length, it demonstrates that, for this range of homopolymer sizes, phase separation is complete: no P4VP homopolymer remains within the PS matrix, in line with the strong incompatibility between PS and P4VP. For PS and PMMA, which have a weaker incompatibility, stable pore sizes as a function of M_w were only found at much higher molecular weights. Additionally, the standard deviations in Figure 7 do not show a trend and

stay in the same order of magnitude, which indicates that the M_w of the homopolymer does not have a significant effect on the pore size distribution as well.

Effect of Rinsing Time

PS(160)-*b*-P4VP(21)/P4VP$_{HP}$(22) films ($f_{P4VP\text{-}HP} = 0.16$) were immersed in ethanol for different durations, in order to investigate the effect of the immersion on the pore size and film morphology.

Figure 8(a) shows that the average pore size and pore size distribution is constant and independent on the immersion treatment. After 10 s (first data point) the average pore size is already 31 ± 9 nm and does not change during the following 2.5 h. This indicates that P4VP$_{HP}$ dissolves rapidly and immersion in ethanol almost instantly creates pores. However, since surface images do not indicate the depth of the pores, it may take longer before all P4VP is washed away and straight-through pores are formed along the whole thickness of the film.

Figure 8(b) shows that the surface porosity increases when the film is immersed in ethanol for a longer time. The porosity is ~9% after 10 s and increases to ~14% in 2.5 h. This is the result of an increase in the number of pores per μm^2 [Fig. 8(c)], which increases from 108 after 10 s to 149 in 2.5 h. Since it is shown that P4VP$_{HP}$ dissolves very rapidly in ethanol, it is not likely that more pores are formed in time because more P4VP$_{HP}$ is washed away. The formation of more pores in time is probably due to situations where BCP P4VP chains swell in time but where rearrangement of the PS matrix is also necessary to create voids.

Effect of Chloroform Vapor Annealing

In order to investigate the effect of a chloroform annealing step on the pore size distribution and film morphology prepared films received a chloroform annealing treatment. Chloroform was chosen as solvent because it is a solvent for both PS and P4VP and can, therefore, mobilize the complete polymer chain. Two routes were evaluated: Solvent vapor annealing prior to pore formation (route 1) and solvent vapor annealing after pore formation (route 2). Figure 9 shows AFM height images of films subjected to vapor annealing for the two routes.

When both routes are compared, no significant change is seen for the first two hours of the annealing treatment. However, after four hours, the morphologies of the films are dramatically different. In the case of solvent vapor annealing prior to pore formation, large circular domains appear on the surface where initially pores were present [Fig. 9(d)]. These dots are no longer pores but instead hollows of several nanometers deep with diameters that are significantly larger than the diameters of the initial pores. In the case of solvent vapor annealing after pore formation, the film is still porous. However, the edges of the pores have become more smooth and in some cases the pores seem to be clogged.

Films have a different structure after four hours of solvent vapor annealing for both routes compared to films that are not exposed to solvent annealing. This indicates that chloroform mobilizes the polymer chains and rearranges the morphology of the films. While thermal or solvent annealing is often used to improve the ordering of equilibrium nanostructures (pure block copolymer films),[22–28] we demonstrate that chloroform solvent annealing is not beneficial for improving the structure of our block copolymer/homopolymer films with nonequilibrium structures.

CONCLUSIONS

Selective removal of a homopolymer from a self-assembling polystyrene-*block*-poly(4-vinyl pyridine) (PS-*b*-P4VP) diblock copolymer and poly(4-vinyl pyridine) (P4VP$_{HP}$) homopolymer film is an easy method to produce isoporous nanoporous films. Nanoporous films were made by spin-coating a block copolymer/homopolymer solution and subsequently immersing the fabricated film in ethanol. Both dissolution of the P4VP homopolymers and swelling of the P4VP block copolymer chain contributed to pore formation. We demonstrate for the first time that even without the addition of homopolymer, immersion in ethanol can still lead to a nanoporous block copolymer film due to swelling of the P4VP chains. Swelling influences pore formation significantly when relatively small pores are formed. Therefore, pore formation not only depends on the content of homopolymers, but also on the solvent and block copolymer type and composition.

Pore sizes can be tuned between 10 and 50 nm by simply varying the homopolymer content and the molecular weight of the block copolymer. Porosities of the films can be tuned between 0.03 and 0.2, and their values depend on the homopolymer content and the duration of immersion in ethanol.

When the average pore size exceeded 30 nm the pore size uniformity is lost as a result of macrophase separation, which limits the range of uniform pore sizes that can be obtained for large BCPs. However, we demonstrate that by using low M_w BCPs, we can obtain excellent pore size control, reach high porosities, while retaining a relatively even pore size distribution. The transition from microphase separation to macrophase separation occurs at lower P4VP$_{HP}$ fractions for larger block copolymers, since larger pores are formed using larger block copolymers.

Varying the molecular weight of homopolymers in a low range (5–22 kg/mol) does not influence the obtained morphology significantly, demonstrating full phase separation of P4VP homopolymers from the PS matrix.

Solvent vapor annealing rearranges the polymers and thereby changes the structure of the films. However, exposing the films to chloroform vapor does not enhance the ordering nor uniformity of the pores. Chloroform vapor annealing prior to immersion in ethanol leads to a nonporous film with only cylindrical domains, while chloroform

vapor annealing after immersion in ethanol leads to a film with a smoother surface and pores with smoother edges.

Because of the presented film characteristics the authors believe that the nanoporous films fabricated in this work are promising for use in ultrafiltration membranes applications. Therefore, the next step will be to fabricate a composite membrane, consisting of a permeable support membrane that provides mechanical strength and our thin BCP layer that provides a high filtering selectivity on top. In this challenging case, our BCP layer will transferred to, or directly coated onto the support membrane.

ACKNOWLEDGMENT

This work is supported by NanoNextNL, a micro and nanotechnology consortium of the Government of The Netherlands and 130 partners.

REFERENCES AND NOTES

1 J. K. Kim, S. Y. Yang, Y. Lee, Y. Kim, *Prog. Polym. Sci. (Oxford)* **2010**, *35*, 1325–1349.

2 F. S. Bates, G. H. Fredrickson, *Phys. Today* **1999**, *52*, 32–38.

3 M. W. Matsen, F. S. Bates, *Macromolecules* **1996**, *29*, 1091–1098.

4 M. W. Matsen, M. Schick, *Phys. Rev. Lett.* **1994**, *72*, 2660–2663.

5 M. A. Shannon, P. W. Bohn, M. Elimelech, J. G. Georgiadis, B. J. Marĩas, A. M. Mayes, *Nature* **2008**, *452*, 301–310.

6 E. A. Jackson, M. A. Hillmyer, *ACS Nano* **2010**, *4*, 3548–3553.

7 M. M. Pendergast, E. M. V. Hoek, *Energy Environ. Sci.* **2011**, *4*, 1946–1971.

8 S. Y. Yang, J. A. Yang, E. S. Kim, G. Jeon, E. J. Oh, K. Y. Choi, S. K. Hahn, J. K. Kim, *ACS Nano* **2010**, *4*, 3817–3822.

9 M.-S. She, R.-M. Ho, *Polymer* **2012**, *53*, 2628–2632.

10 Y. S. Jung, C. A. Ross, *Small* **2009**, *5*, 1654–1659.

11 C.-C. Chao, T.-C. Wang, R.-M. Ho, P. Georgopanos, A. Avgeropoulos, E. L. Thomas, *ACS Nano* **2010**, *4*, 2088–2094.

12 B. P. Bastakoti, Y.-C. Hsu, S.-H. Liao, K. C. W. Wu, M. Inoue, S.-i. Yusa, K. Nakashima, Y. Yamauchi, *Chem. Asian J.* **2013**, *8*, 1301–1305.

13 B. P. Bastakoti, S. Ishihara, S.-Y. Leo, K. Ariga, K. C. W. Wu, Y. Yamauchi, *Langmuir* **2014**, *30*, 651–659.

14 B. P. Bastakoti, N. L. Torad, Y. Yamauchi, *ACS Appl. Mater. Interfaces* **2013**, *6*, 854–860.

15 W. A. Phillip, B. O'Neill, M. Rodwogin, M. A. Hillmyer, E. L. Cussler, *ACS Appl. Mater. Interfaces* **2010**, *2*, 847–853.

16 T. Thurn-Albrecht, R. Steiner, J. DeRouchey, C. M. Stafford, E. Huang, M. Bal, M. Tuominen, C. J. Hawker, T. P. Russell, *Adv. Mater.* **2000**, *12*, 787–791.

17 S. Y. Yang, J. Park, J. Yoon, M. Ree, S. K. Jang, J. K. Kim, *Adv. Funct. Mater.* **2008**, *18*, 1371–1377.

18 S. E. Querelle, E. A. Jackson, E. L. Cussler, M. A. Hillmyer, *ACS Appl. Mater. Interfaces* **2013**, *5*, 5044–5050.

19 E. A. Jackson, Y. Lee, M. A. Hillmyer, *Macromolecules* **2013**, *46*, 1484–1491.

20 J. Bolton, T. S. Bailey, J. Rzayev, *Nano Lett.* **2011**, *11*, 998–1001.

21 L. Lei, Y. Xia, X. Chen, S. Shi, *J. Appl. Polym. Sci.* **2014**, *131*, 39638.

22 S. O'Driscoll, G. Demirel, R. A. Farrell, T. G. Fitzgerald, C. O'Mahony, J. D. Holmes, M. A. Morris, *Polym. Adv. Technol.* **2011**, *22*, 915–923.

23 H. Y. Si, J. S. Chen, G. M. Chow, *Colloids Surf. A Physicochem. Eng. Aspects* **2011**, *373*, 82–87.

24 C. Sinturel, M. Vayer, M. Morris, M. A. Hillmyer, *Macromolecules* **2013**, *46*, 5399–5415.

25 J. Zhao, S. Jiang, X. Ji, L. An, B. Jiang, *Polymer* **2005**, *46*, 6513–6521.

26 S. Wu, C. Bubeck, *Macromolecules* **2013**, *46*, 3512–3518.

27 W. van Zoelen, T. Asumaa, J. Ruokolainen, O. Ikkala, G. ten Brinke, *Macromolecules* **2008**, *41*, 3199–3208.

28 G. Kim, M. Libera, *Macromolecules* **1998**, *31*, 2569–2577.

29 S. H. Kim, M. J. Misner, T. P. Russell, *Adv. Mater.* **2004**, *16*, 2119–2123.

30 K. Koo, H. Ahn, S.-W. Kim, D. Y. Ryu, T. P. Russell, *Soft Matter* **2013**, *9*, 9059–9071.

31 S. P. Nunes, M. Karunakaran, N. Pradeep, A. R. Behzad, B. Hooghan, R. Sougrat, H. He, K. V. Peinemann, *Langmuir* **2011**, *27*, 10184–10190.

32 S. P. Nunes, R. Sougrat, B. Hooghan, D. H. Anjum, A. R. Behzad, L. Zhao, N. Pradeep, I. Pinnau, U. Vainio, K. V. Peinemann, *Macromolecules* **2010**, *43*, 8079–8085.

33 K. V. Peinemann, V. Abetz, P. F. W. Simon, *Nat. Mater.* **2007**, *6*, 992–996.

34 M. Radjabian, J. Koll, K. Buhr, U. A. Handge, V. Abetz, *Polymer* **2013**, *54*, 1803–1812.

35 M. Mulder, Basic principles of membrane technology, Kluwer Academic Publishers: Dordrecht, **1996**.

36 W. Lee, X. Zhang, R. M. Briber, *Polymer* **2010**, *51*, 2376–2382.

37 I. Vukovic, S. Punzhin, Z. Vukovic, P. Onck, J. T. M. De Hosson, G. Ten Brinke, K. Loos, *ACS Nano* **2011**, *5*, 6339–6348.

38 X. Li, C. A. Fustin, N. Lefèvre, J. F. Gohy, S. D. Feyter, J. D. Baerdemaeker, W. Egger, I. F. J. Vankelecom, *J. Mater. Chem.* **2010**, *20*, 4333–4339.

39 S. Y. Yang, I. Ryu, H. Y. Kim, J. K. Kim, S. K. Jang, T. P. Russell, *Adv. Mater.* **2006**, *18*, 709–712.

40 U. Jeong, H. C. Kim, R. L. Rodriguez, I. Y. Tsai, C. M. Stafford, J. K. Kim, C. J. Hawker, T. P. Russell, *Adv. Mater.* **2002**, *14*, 274–276.

41 U. Jeong, D. Y. Ryu, D. H. Kho, J. K. Kim, J. T. Goldbach, D. H. Kim, T. P. Russell, *Adv. Mater.* **2004**, *16*, 533–536.

42 J. Ruokolainen, M. Saariaho, O. Ikkala, G. ten Brinke, E. L. Thomas, M. Torkkeli, R. Serimaa, *Macromolecules* **1999**, *32*, 1152–1158.

43 D. H. Kim, K. H. A. Lau, W. Joo, J. Peng, U. Jeong, C. J. Hawker, J. K. Kim, T. P. Russell, W. Knoll, *J. Phys. Chem. B* **2006**, *110*, 15381–15388.

44 H. Kitano, S. Akasaka, T. Inoue, F. Chen, M. Takenaka, H. Hasegawa, H. Yoshida, H. Nagano, *Langmuir* **2007**, *23*, 6404–6410.

45 J. K. Lee, J. S. Kim, H. J. Lim, K. H. Lee, S. M. Jo, T. Ougizawa, *Polymer* **2006**, *47*, 5420–5428.

46 X. Li, S. Zhao, S. Zhang, D. H. Kim, W. Knoll, *Langmuir* **2007**, *23*, 6883–6888.

47 D. H. Park, *Nanotechnology* **2007**, *18*, 355304.

48 W. Joo, S. Y. Yang, J. K. Kim, H. Jinnai, *Langmuir* **2008**, *24*, 12612–12617.

49 H. Tanaka, T. Hashimoto, *Macromolecules* **1991**, *24*, 5713–5720.

50 T. Hashimoto, S. Koizumi, H. Hasegawa, T. Izumitani, S. T. Hyde, *Macromolecules* **1992**, *25*, 1433–1439.

51 S. Koizumi, H. Hasegawa, T. Hashimoto, *Macromolecules* **1994**, *27*, 6532–6540.

52 N. Y. Vaidya, C. D. Han, D. Kim, N. Sakamoto, T. Hashimoto, *Macromolecules* **2000**, *34*, 222–234.

53 H. Ahn, Y. Lee, H. Lee, S. Park, Y. Kim, J. Cho, D. Y. Ryu, *Polymer* **2012**, *53*, 5163–5169.

54 U. Jeong, D. Y. Ryu, J. K. Kim, D. H. Kim, X. Wu, T. P. Russell, *Macromolecules* **2003**, *36*, 10126–10129.

55 U. Jeong, D. Y. Ryu, D. H. Kho, D. H. Lee, J. K. Kim, T. P. Russell, *Macromolecules* **2003**, *36*, 3626–3634.

56 B. K. Kuila, M. Stamm, *Macromolecular Symposia* **2011**, *303*, 85–94.

57 S. Roland, D. Gaspard, R. E. Prud'homme, C. G. Bazuin, *Macromolecules* **2012**, *45*, 5463–5476.

58 C. M. Hansen, Hansen Solubility Parameters: A User's Handbook, CRC Press: Boca Raton, **2000**.

59 S. Liu, L. Wang, B. Liu, Y. Song, *Polymer* **2013**, *54*, 3065–3070.